Nonvolatile Resistive Switching Memory Properties of Thermally Annealed Titania Precursor/Polyelectrolyte Multilayers

Chanwoo Lee,[†] Inpyo Kim,[†] Hyunjung Shin,[†] Sanghyo Kim,[‡] and Jinhan Cho*,[†]

[†]*School of Advanced Materials Engineering, Kookmin University, Jeongneung-dong, Seongbuk-gu, Seoul 136-702, South Korea, and* [‡]*College of BioNano Technology, Kyungwon University, San 65, Bokjeong-dong, Sujeong-gu, Kwonggi-do 461-701 Korea*

Received July 20, 2009. Revised Manuscript Received August 17, 2009

We describe a novel and versatile approach for preparing resistive switching memory devices based on transition metal oxides. A titania precursor and poly(allyamine hydrochloride) (PAH) layers were deposited alternately onto platinum (Pt)-coated silicon substrates using electrostatic interactions. The multilayers were then converted to TiO_2 nanocomposite (TiO_2 NC) films after thermal annealing. A top electrode was coated on the TiO_2 NC films to complete device fabrication. When an external bias was applied to the devices, a switching phenomenon independent of the voltage polarity (i.e., unipolar switching) was observed at low operating voltages (approximately 0.4 V_{RESET} and 1.3 V_{SET}), which is comparable to that observed in conventional devices fabricated by sputtering or metal organic chemical vapor deposition processes. The reported approach offers new opportunities for preparing inorganic material-based resistive switching memory devices with tailored electronic properties, allowing facile solution processing.

Introduction

Nonvolatile resistive switching memory (RSM) devices have attracted considerable interest as a result of the widespread use of mobile electronics.[1−3] In particular, RSM devices based on binary transition metal oxides (TMOs), which exhibit excellent device performance (i.e., rapid switching speed and high ON/OFF ratio) with a simple device structure,[4−8] are notable candidates for the next generation of nonvolatile memory devices. However, preparing large-area devices at low cost with a simplified manufacturing process is quite difficult when conventional sputtering or metal organic chemical vapor deposition processes are used to prepare TMO films, even though inorganic materials have excellent thermal stability and durability in air. Recently, it was reported that perovskite magnetites (e.g., $La_{1−x}Ca_xMnO_3$), doped perovskite oxides (e.g., Mo-doped $SrZrO_3$), and binary TMO (e.g., TiO_2) prepared by sol−gel solution processes instead of vacuum deposition can show resistive switching characteristics.[9−12] As another approach, soluble polymers, such as semiconducting,[13] conducting polymers,[14] or nanocomposites composed of conducting components (i.e., metal nanoparticles, quantum dots, or carbon nanotube)[15−18] and insulating polymers,[19] may be promising candidates as the active layers in the next generation of nonvolatile memory devices because they can be deposited by spin-coating.[5−8,20]

Among the various solution deposition methods available, the layer-by-layer (LbL) assembly method based on a solution dipping process was reported to be quite useful for preparing organic and/or inorganic nanocomposite films with tailored electrical properties and layer thickness as well as various functional components on substrates with different sizes and shape.[21−28] Spin-coating methods can be applied to flat substrates with a limited large size, even though it can allow the coating of active materials onto substrates larger than those prepared using vacuum deposition methods. Furthermore, LbL assembly can be achieved by tuning the complementary (electrostatic, hydrogen-bonding, or covalent bonding) interactions. Recently, the Advincula group reported that nanometer-scale charging in LbL films based on conjugated polymers can provide a write−read device using current-sensing atomic force microscopy (CS-AFM).[24] Quite recently, the Pal group reported that electrostatic assembled multilayers composed of CdSe quantum dots can show

*Corresponding author. E-mail: jinhan@kookmin.ac.kr.
(1) Waser, R.; Aono, M. *Nat. Mater.* **2007**, *6*, 833.
(2) Weitz, R. T.; Walter, A.; Engl, R.; Sezi, R.; Dehm, C. *Nano Lett.* **2006**, *6*, 2810.
(3) Jo, S. H.; Kim, K.-H.; Lu, W. *Nano Lett.* **2009**, *9*, 496.
(4) Hickmott, T. W. *J. Appl. Phys.* **1962**, *33*, 2669.
(5) Choi, S.; Hong, S.-H.; Cho, S. H.; Park, S.; Park, S.-M.; Kim, O.; Ree, M. *Adv. Mater.* **2008**, *20*, 1766.
(6) Yang, Y.; Ouyang, J.; Ma, L.; Tseng, R. J.-H.; Chu, C.-W. *Adv. Funct. Mater.* **2006**, *16*, 1001.
(7) Lauters, M.; McCarthy, B.; Sarid, D.; Jabbour, G. E. *Appl. Phys. Lett.* **2006**, *89*, 013507.
(8) Majumdar, H. S.; Bandyopadhyay, A.; Bolognesi, A.; Pal, A. J. *J. Appl. Phys.* **2002**, *91*, 2433.
(9) Zhang, T.; Su, Z.; Chen, H.; Ding, L.; Zhang, W. *Appl. Phys. Lett.* **2008**, *93*, 172104.
(10) Lin, C.-Y.; Lin, C.-C.; Huang, C.-H.; Lin, C.-H.; Tseng, T.-Y. *Surf. Coat. Technol.* **2007**, *202*, 1319–1322.
(11) Szot, K.; Speier, W.; Bihlmayer, G.; Waser, R. *Nat. Mater.* **2006**, *5*, 312.
(12) Lee, C.; Kim, I.; Choi, W.; Shin, H.; Cho, J. *Langmuir* **2009**, *25*, 4274.
(13) Baek, S.; Lee, D.; Kim, J.; Hong, S.-H.; Kim, O.; Ree, M. *Adv. Funct. Mater.* **2008**, *17*, 2637.
(14) Barman, S.; Deng, F.; McCreery, R. C. *J. Am. Chem. Soc.* **2008**, *130*, 11073.

(15) Guan, W.; Long, S.; Jia, R.; Liu, M. *Appl. Phys. Lett.* **2007**, *91*, 062111.
(16) Das, B. C.; Batabyal, S. K.; Pal, A. J. *Adv. Mater.* **2007**, *19*, 4172.
(17) Rueckes, T.; Kim, K.; Joselevich, E.; Tseng, G. Y.; Cheung, C.-L.; Lieber, C. M. *Science* **2000**, *289*, 94.
(18) Verbakel, F.; Meskers, S. C. J.; Janssen, R. A. J. *Chem. Mater.* **2006**, *18*, 2707.
(19) Verbakel, F.; Meskers, S. C. J.; de Leeuw, D. M.; Janssen, R. A. J. *J. Phys. Chem. C* **2008**, *112*, 5254.
(20) Bozano, L. D.; Kean, B. W.; Beinhoff, M.; Carter, K. R.; Rice, P. M.; Scott, J. C. *Adv. Funct. Mater.* **2005**, *15*, 1933.
(21) Decher, G. *Science* **1997**, *277*, 1232.
(22) Caruso, F.; Caruso, R. A.; Möhwald, H. *Science* **1998**, *282*, 1111.
(23) Zhang, X.; Shi, F.; Yu, X.; Liu, H.; Fu, Y.; Wang, Z.; Jiang, L.; Li, X. *J. Am. Chem. Soc.* **2004**, *126*, 3064.
(24) Jiang, G.; Baba, A.; Advincula, R. *Langmuir* **2007**, *23*, 817.
(25) Das, B. C.; Batabyal, S. K.; Pal, A. J. *Adv. Mater.* **2007**, *19*, 4172.
(26) Lee, J.-S.; Cho, J.; Lee, C.; Kim, I.; Park, J.; Kim, Y.; Shin, H.; Lee, J.; Caruso, F. *Nat. Nanotechnol.* **2007**, *2*, 790.
(27) Caruso, F.; Shi, X.; Caruso, R. A.; Susha, A. *Adv. Mater.* **2001**, *13*, 740.
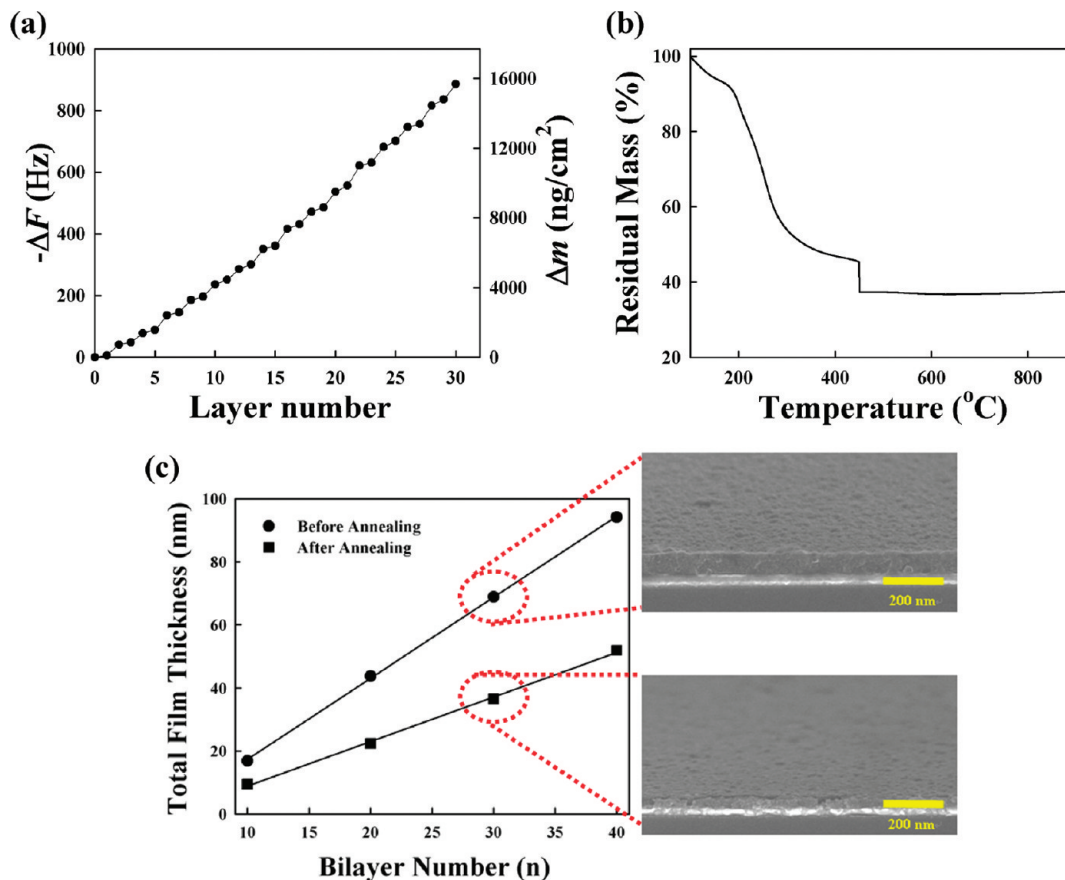(28) Caruso, R. A.; Susha, A.; Caruso, F. *Chem. Mater.* **2001**, *13*, 400.

Figure 1. (a) Frequency and mass change of PAH/TALH multilayers measured with increasing layer number from 1 to 30. In this case, the mass change per unit area was calculated from frequency change. (b) Thermogravimetric analysis of aggregated PAH/TALH powder with the mass ratio of about 1:5. The inset indicates the change in residual mass of aggregated powder during the isothermal process (at 450 °C for 4 h). The heating rate of TGA was 10 °C/min. (c) Film thicknesses and SEM images of (PAH/TALH)$_n$ multilayers before and after thermal treatment at 450 °C for 6 h (2 h in nitrogen and 4 h in oxygen condition).

electrical bistability.[25] As another example, it was reported by our group that LbL multilayers containing metal nanoparticles can be used as charge-trap flash memory devices with operation system and physics quite different from that of RSM devices.[26]

In this study, the LbL approach was used to assemble titania precursor/poly(allylamine hydrochloride) (PAH) multilayer films on platinum (Pt) electrodes in order to prepare TiO$_2$ nanocomposite (TiO$_2$ NC) devices with a tailored nanostructure and resistive switching phenomena after a thermal treatment. Although the Caruso group reported that LbL-assembled multilayers composed of cationic PAH and anionic titanium(IV) bis(ammonium lactato) dihydroxide (TALH) could be converted easily to TiO$_2$ nanocomposites after thermal conversion,[27,28] the motivation of the present study was to fabricate the inorganic material-based nonvolatile memory cells via the thermal conversion of PAH/TALH nanocomposite multilayers. This work highlights the fact that large−area inorganic oxide-based memory devices can be fabricated easily by a solution dipping process, and that the electrical performance of the resulting devices is comparable to that of conventional inorganic RSM devices produced by vacuum deposition. It is believed that this approach can be used in many potential electronic applications requiring high performance, long durability, large-area and solution processing in air.

Experimental Sections

Preparation of TiO$_2$ NC Films from (PAH/TALH)$_n$ Multilayers. The concentration of PAH (M_w = 70 000, Aldrich) and TALH (Aldrich) solutions used in all experiments was 1 and 50 mg·mL^{-1}, respectively. Figure S1a in the Supporting Information shows the structure of the materials used. Pt-coated Si substrates had an anionic surface by irradiating UV light. These substrates were first dipped for 10 min in a cationic PAH solution (containing 0.5 M NaCl), washed twice by dipping in water for 1 min, and air-dried with a gentle stream of nitrogen. Anionic TALH was then deposited onto the PAH-coated substrates using the same adsorption, washing, and drying procedures, as described above. The resulting multilayer films were annealed thermally at 450 °C for 2 h under nitrogen and then annealed at the same temperature for 4 h under oxygen conditions.

Thermogravimetric Analysis of PAH/TALH Nanocomposites. To confirm the thermal decomposition of the PAH/TALH multilayers, the electrostatically aggregated PAH/TALH powder was first prepared at a mass ratio of approximately PAH/TALH = 1: 5 in an aqueous solution (the mass ratio of the powder was determined from the amount of PAH (i.e., Δm of ∼141 ng·cm^{-2}) and TALH (i.e., Δm of ∼724 ng·cm^{-2}) adsorbed in the LbL multilayers; see the quartz crystal microgravimetry (QCM) results). The aggregated powder was heated to 450 °C at a heating rate of 5 °C·min and annealed at that temperature for 4 h. It should be noted that this thermal process for the powder is similar to that used for the LbL multilayers. After an isothermal treatment for 4 h, the powder was heated to 900 °C to determine the presence of any residual organic material.

QCM Measurements. A QCM device (QCM200, SRS) was used to measure the mass of the material deposited after each adsorption step. The resonance frequency of the QCM electrodes was approximately 5 MHz. The adsorbed mass of PAH and TALH, Δm, can be calculated from the change in QCM
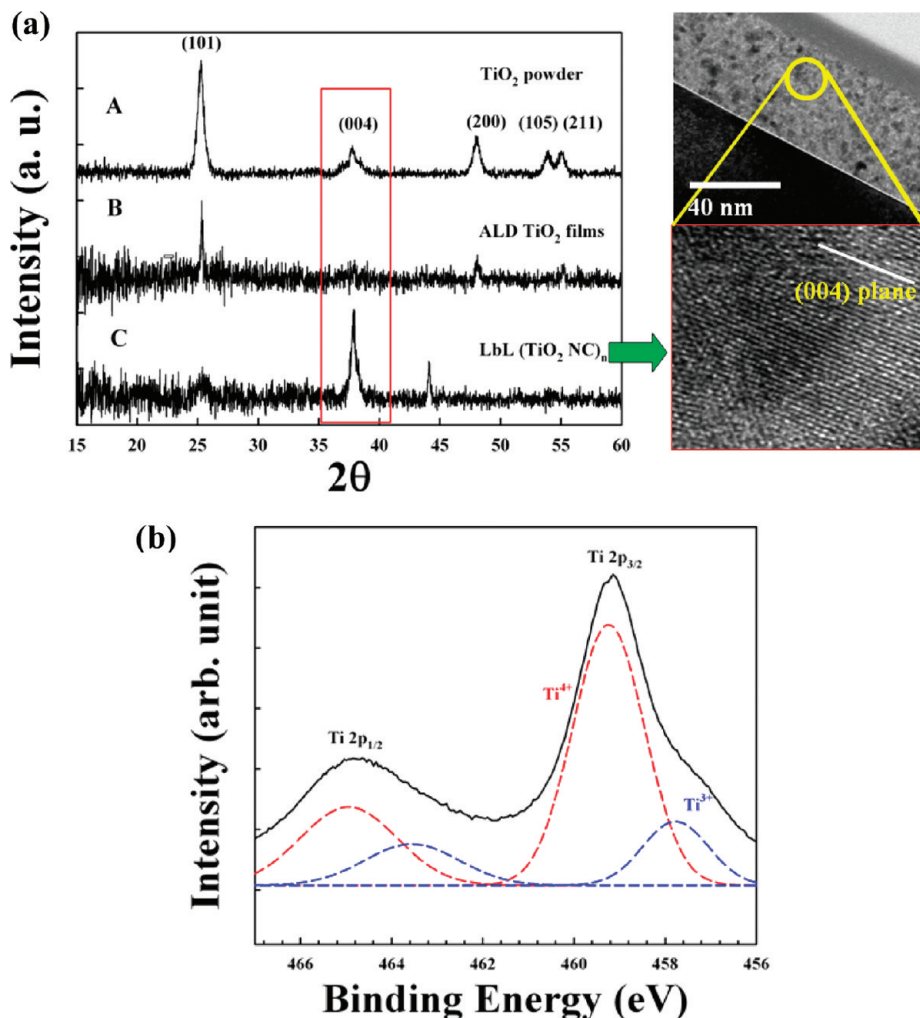
Figure 2. (a) XRD patterns of TiO_2 powder prepared from TALH (A), atomic layer deposited TiO_2 films (B), and LbL TiO_2 NC multilayers (C). Three different samples are thermally annealed at 450 °C for 6 h in nitrogen (2 h) and subsequent oxygen (4 h) condition. The cross-sectional TEM images of TiO_2 NC multilayers indicate the crystalline structure. (b) XPS spectra of LbL TiO_2 NC multilayers. Ti(2p) spectrum was deconvoluted into two spin−orbit components (Ti^{4+} and Ti^{3+}).

frequency, ΔF, using the Sauerbrey equation: $\Delta F\,(Hz) = -56.6 \times \Delta m_A$, where Δm_A is the mass change per quartz crystal unit area in micrograms per square centimeter ($\mu g \cdot cm^{-2}$).

Surface Morphology. The surface morphology and roughness of the thermally annealed TiO_2 NC on Si substrates were measured by AFM in tapping mode (SPA400, SEIKO).

Crystal Structure and Chemical Compositions. The crystal structure of LbL TiO_2 NC was examined by X-ray diffraction (XRD) at room temperature. Data collection was performed from 15 to 60° 2θ using Cu Kα radiation ($\lambda = 1.54$ Å, model: Bruker D8 Discover, Germany). Cross-section transmission electron spectroscopy (TEM, model: JEOL 300 kV) was also used to analyze the TiO_2 crystal structure as well as the internal structure of the nanocomposite multilayers. X-ray photoelectron spectroscopy (XPS, Sigma Probe) was performed to determine the binding state of Ti ions and the presence of residual carbon.

Fabrication of RSM Devices. All samples were prepared on Si substrates (2 cm × 2 cm) with a SiO_2 layer of approximately 100 nm. A Ti layer, 20 nm in thickness, was then deposited on the substrates, and a bottom electrode (Pt) was subsequently deposited by DC-magnetron sputtering. The $(PAH/TALH)_n$ multilayer films were then formed on the Pt-coated Si substrates. The resulting multilayer films were thermally annealed at 450 °C for 2 h under nitrogen followed by subsequent annealing at the same temperature for 4 h under oxygen condition. After thermal conversion, 100 μm diameter thick top electrodes (Ag) were deposited onto the
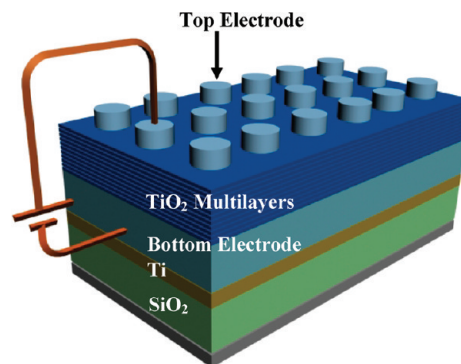

Figure 3. Schematic for RSM devices based on TiO_2 NC multilayers, $(TiO_2\ NC)_n$.

nanocomposite films. To investigate the resistive switching behavior of the LbL multilayered devices, the current−voltage ($I-V$) curves were measured using a semiconductor parametric analyzer (SPA, Agilent 4155B) in air environment. The pulsed voltage duration dependence of the high and low current states was investigated using a semiconductor parametric analyzer (HP 4155A) and a pulse generator (Agilent 81104A). *Although Ag electrodes were used as the top electrodes in these devices, similar switching behavior was also observed using Pt or tungsten top electrodes. This suggests that the Ag*
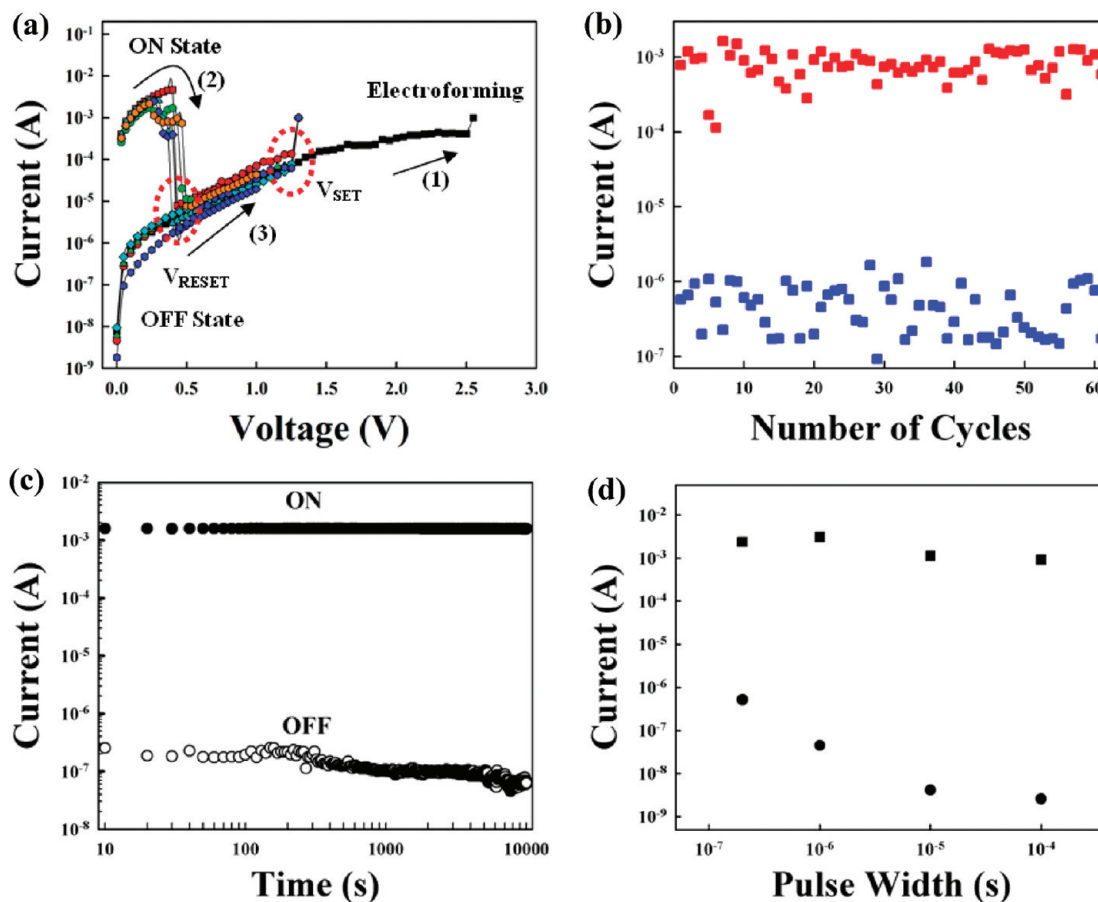
Figure 4. (a) $I-V$ curves of $(TiO_2\ NC)_{30}$ multilayer device showing repetitive switching cycles after initial electroforming process. (b) Cycling and (c) retention time test of $(TiO_2\ NC)_{30}$ multilayer device. The high and low conductive states were induced using a reading voltage of 0.1 V. (d) The ON current values at 3.5 V and OFF current values at 1 V for different pulse widths (200 ns, 1 μs, 10 and 100 μs).

electrode itself has no significant effect on the resistive switching characteristics of LbL TiO₂ NC.

CS-AFM. Local current maps on the nanoscale were measured using current sensing CS-AFM (e-sweep, SEIKO). For the CS-AFM measurements, the CS-AFM tip (i.e., Pt tip) was used as the top electrode instead of the Ag electrode.

Results and Discussion

QCM was performed to measure the amount of PAH and TALH adsorbed in the multilayer films. Figure 1 shows the frequency changes, $-\Delta F$, and mass changes in the adsorbed PAH and TALH with increasing number of layers. The changes in mass were calculated from the changes in frequency using the Sauerbrey equation (see the Experimental Section). These QCM frequency (or mass) changes suggest that regular multilayer film growth occurs when TALH and organic PAH are assembled LbL from the deposition solutions. The alternate deposition of PAH and TALH resulted in a $-\Delta F$ of 8 ± 2 (Δm of ~ 141 ng·cm^{-2}) and 41 ± 4 Hz (Δm of ~ 724 ng·cm^{-2}), respectively. The PAH/TALH multilayers were converted easily to TiO₂ NC multilayer films when annealed at 450 °C, while the PAH (thermal degradation temperature of PAH $\approx$ 240 °C) and TALH layers underwent thermal degradation. As shown in Figure 1b, the TALH/PAH nanocomposites with the isothermal treatment at 450 °C showed an almost negligible decrease in residual mass between 450 and 900 °C. The total film thickness of the TiO₂ NC layer was decreased to approximately 53% of the initial film thickness (Figure 1c), and these films were quite homogeneous (see Supporting Information, Figure S1b).

XRD and cross-sectional high-resolution TEM (HR-TEM) were also used to examine the formation and crystalline structure of the TiO₂ NC layers after annealing. As shown in Figure 2a, the XRD patterns of the TiO₂ powder prepared from the thermally annealed TALH and TiO₂ films grown by atomic layer deposition had an evident (101) peak along with a relatively weak (004) peak typical of anatase crystals. On the other hand, LbL TiO₂ NC had a strong anatase (004) peak and relatively weak anatase (101) and rutile crystal (210) peaks. The structure of the LbL TiO₂ films is closely related to the crystalline growth of TALH layers confined between the adjacent PAH layers. HR-TEM confirmed the formation of (004) TiO₂ (lattice spacing: 2.378 Å) within the nanocomposite films. The in situ change in crystalline state, stacking and periodicity of the films during thermal annealing was not examined due to the limited capacity of the equipment. However, such an in situ investigation will provide more information on the formation and crystalline structure of TiO₂ NC films.

Furthermore, the chemical compositions within the LbL TiO₂ films were analyzed by XPS (Figure 2b). The initial thermal annealing process in nitrogen conditions can induce oxygen deficiencies accompanied by an increase in the local electron concentration. This oxygen deficient state can be confirmed by the Ti2p$_{3/2}$ peak shifting to a lower binding energy due to the presence of Ti^{3+} ions.[12,29,30] The Ti(2p) spectrum was examined further to

(29) Knauth, P.; Tuller, H. L. *J. Appl. Phys.* **1999**, *85*, 897.

(30) *NIST X-ray Photoelectron Spectroscopy Database 20*, version 3.5 (Web version); Wagner, C. D., Naumkin, A. V., Kraut-Vass, A., Allison, J. W., Powell, C. J., Rumble, J. R., Eds. National Institute of Standards and Technology: Gaithersburg, MD, **2003**.
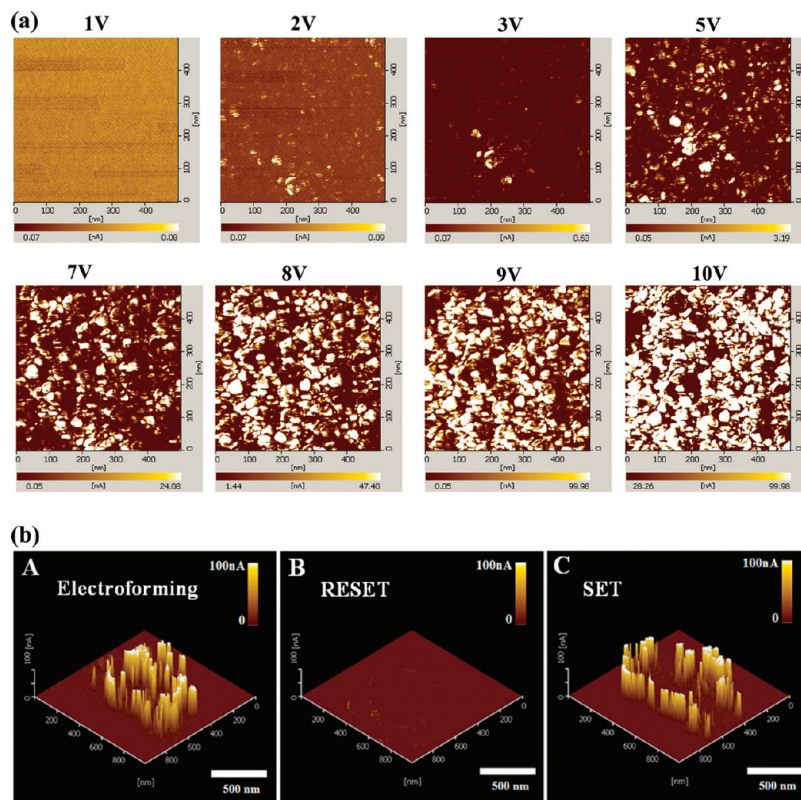
Figure 5. (a) CS-AFM images of TiO_2 NC multilayers measured with increasing initial electroforming voltage. It was observed that the number of conductive filaments sharply increased with increasing the applied voltage. (b) CS-AFM images of TiO_2 NC multilayers after electroforming (A) of 8 V, V_{RESET} (B) of 3 V and V_{SET} (C) of 5 V, respectively.

demonstrate the generation of oxygen vacancies within the LbL TiO_2 films. The measured spectrum can be resolved into two spin−orbit components, which are identified as Ti^{4+} (459.2 eV) and Ti^{3+} (457.8 eV).[12,30] LbL TiO_2 multilayers can operated as an efficient active layer in RSM devices considering that the presence of Ti^{3+} acts as an n-type dopant, transforming an insulating oxide into an electrically conducting semiconductor. Furthermore, TiO_2 NC films should be considered as simple single-layered TiO_2 films with material-based defects, instead of a multilayer structure with a complex geometry because the PAH layers inserted between the neighboring TALH are decomposed thermally by annealing.

A RSM device composed of TiO_2 NC films was fabricated based on these results (Figure 3). The electrical measurements were operated at an applied voltage pulse with a 1 μs width in air. For simplicity, a positive electric field is defined when a positive voltage is applied to the top electrode. Figure 4a shows the current−voltage ($I-V$) curves of a 30 bilayered TiO_2 NC film (thickness approximately 40 nm) undergoing unipolar switching behavior (i.e., the switching behavior independent of voltage polarity) under a positive electric field. During the first sweep of the applied positive voltage to the top electrode, the device showed an abrupt increase in current at approximately 2.5 V (e.g., electroforming stage, region 1 in Figure 4a). In this case, the current compliance was limited to 1 mA in order to prevent total dielectric breakdown of the device from overcurrent. The high current state ('ON' state) formed after the initial electroforming process with current compliance returned to the low current state with a sharp decrease in current at approximately 0.4 V (i.e., RESET voltage, V_{RESET}) during the second voltage sweep (from 0 to approximately 1.0 V) (e.g., from the ON state to the RESET state, region 2). When the applied voltage was increased from 0 V

to 1.4 V (e.g., region 3), the device with the low current state ("OFF" state) showed an abrupt increase in current at approximately 1.3 V (i.e., SET voltage, V_{SET}). Although these processes were repeated continuously, the change in V_{RESET} and V_{SET} was narrow. This suggests that the electrical operation of these multilayered devices is quite stable. The electrical properties of RSM devices were also investigated with three different sizes of top electrodes (i.e., 5, 100, and 500 μm diameter). In this case, there was no significant difference in the RESET or SET current level between these devices. Although it was reported that the significant scaling down of the cell size from 100 to 0.01 μm^2 could result in a decrease in RESET current of less than 1 order of magnitude, it was difficult to scale down the top electrodes to ∼100 nm used in this study due to the limited capacity of the laboratory equipment.

The V_{RESET} and V_{SET} of approximately 0.4 and 1.3 V, respectively, are lower operating voltages than the approximately 1 and 2 V, respectively, generally observed for conventional unipolar switching devices. These low operating voltages of the devices prepared from the thermal decomposition of organometallic materials were attributed the presence of a relatively large amount of material-based defects, such as an oxygen deficiency state or grain boundary compared to those of sputtered TiO_2 devices, even though the mechanism is not completely understood. In addition, the multilayer thickness has a significant effect on the operating voltages. Specifically, the RESET and SET voltages of LbL RSM devices increased with increasing film thickness (see Supporting Information, Figure S2). However, the electrical properties of devices made from the 10 (12 nm thickness) and 20 bilayered film (approxiamtely 25 nm thickness) were unstable. Our devices also exhibited unipolar switching behavior (V_{RESET} and V_{SET} of approximately −0.5 V and −1.3 V,

respectively) in the direction of the negative voltage sweep (see Supporting Information, Figure S3).

A cycling and retention time test of 30 bilayered TiO_2 NC devices was carried out to determine their electrical stability in the ON and OFF states using a reading voltage of 0.1 V (Figure 4b,c). In these cases, the ON and OFF states were maintained during the repeated cycling tests and test period of 10^4 s. The ON and OFF states were monitored as a function of the pulsed voltage duration (τ_p) with a pulse height of 3.5 and 1 V, respectively, as shown in Figure 4d. The ON/OFF current ratio increased from $\sim 10^3$ to $\sim 10^6$ with increasing τ_p from 200 ns to 100 μs. These reversible switching properties were maintained for at least 7 months, demonstrating their excellent electrical stability.

Furthermore, the local current images during the repetitive switching cycles of the devices were examined on the nanometer scale by CS-AFM. In this case, localized conducting paths were formed randomly at an electroforming voltage between 2 and 10 V. Above 10 V, the films lost their reversible switching properties as a result of dielectric breakdown (Figure 5a). Therefore, the V_{RESET}, V_{SET}, and electroforming voltages were adjusted for device operation on the nanometer scale based on these electrical characteristics (Figure 5b). The formation and rupture of the randomly distributed paths were observed from the electroforming, RESET, and SET processes. This suggests that the current density between the top and bottom electrode is not uniform but concentrated in these localized conducting paths, which are turned on and off during switching. In addition, the measured V_{RESET} and V_{SET} of 3 and 5 V, respectively, were higher than those from the devices shown in Figure 4a. Although not completely understood, it is believed that the surface interfacial contamination on conducting AFM surfaces may provide an additional energy barrier for the increased voltage thresholds for SET and RESET. Furthermore, the possibility that the electric field exerted from the tip is nonuniform throughout the TiO_2 layer cannot be excluded because the conducting AFM tip can operate as an electrical point source. This nonuniform electric field can increase the applied voltages for resistive switching.[12]

The unipolar switching behavior observed from these devices can be described as a conducting filamentary model of fuse-antifuse type based on local Joule heating.[3,31] This means that the reversible formation (high current state) and disruption (low current state) of the conducting filamentary path within the oxide layers under an applied voltage is caused by voltage-induced partial dielectric breakdown and thermal breakdown at higher voltages, respectively. As a result, material-based defects in these devices, such as oxygen-deficienies, can have a significant effect on the formation and disruption of local conducting filamentary paths at low operating voltages and low electroforming voltages.

Conclusion

RSM devices based on TMOs were prepared from LbL-assembled multilayer films. The TiO_2 NC devices showed low electroforming (2.6 V) and operating voltages (i.e., $V_{RESET} \sim 0.4 \pm 0.2$ V and $V_{SET} \sim 1.2 \pm 0.2$ V) with an ON/OFF ratio of $\sim 10^3$. The importance of this work lies in the fact that this approach is based on an LbL assembly method using solution-processable inorganic precursors, which allows the production of large-area inorganic oxide-based devices with excellent device performance.

Supporting Information Available: Molecular structure of PAH and TALH; AFM image of TiO_2 NC multilayers; $I-V$ curves of TiO_2 NC films. This material is available free of charge via the Internet at http://pubs.acs.org.

(31) Schindler, C.; S. C. P. Thermadam, S. C. P.; Waser, R.; Kozicki, M. N. *IEEE Trans. Electron Devices* **2007**, *54*, 2762.